Experimental Realization of Stable Exceptional Chains Protected by Non-Hermitian Latent Symmetries Unique to Mechanical Systems

Xiaohan Cui,[1,*] Ruo-Yang Zhang,[1,*] Xulong Wang,[2] Wei Wang,[2] Guancong Ma,[2,†] and C. T. Chan[1,‡]
[1]Department of Physics, The Hong Kong University of Science and Technology, Hong Kong, China
[2]Department of Physics, Hong Kong Baptist University, Kowloon Tong, Hong Kong, China

(Received 20 April 2023; revised 20 August 2023; accepted 8 November 2023; published 7 December 2023)

Lines of exceptional points are robust in the three-dimensional non-Hermitian parameter space without requiring any symmetry. However, when more elaborate exceptional structures are considered, the role of symmetry becomes critical. One such case is the exceptional chain (EC), which is formed by the intersection or osculation of multiple exceptional lines (ELs). In this Letter, we investigate a non-Hermitian classical mechanical system and reveal that a symmetry intrinsic to second-order dynamical equations, in combination with the source-free principle of ELs, guarantees the emergence of ECs. This symmetry can be understood as a non-Hermitian generalized latent symmetry, which is absent in prevailing formalisms rooted in first-order Schrödinger-like equations and has largely been overlooked so far. We experimentally confirm and characterize the ECs using an active mechanical oscillator system. Moreover, by measuring eigenvalue braiding around the ELs meeting at a chain point, we demonstrate the source-free principle of directed ELs that underlies the mechanism for EC formation. Our Letter not only enriches the diversity of non-Hermitian exceptional point configurations, but also highlights the new potential for non-Hermitian physics in second-order dynamical systems.

DOI: 10.1103/PhysRevLett.131.237201

Introduction.—Pioneered by the study of topological insulators in electronic systems [1,2], topology has brought a conceptual revolution sweeping across diverse fields of physics, including classical wave systems such as photonics [3,4], acoustics [5,6], and elastic waves [7–12]. On a different frontier, the development of non-Hermitian physics has recently been merging with topological phases [13–19]. Because of the experimental advantages, classical systems are becoming powerful test beds for non-Hermitian topological phenomena [20–33]. Exceptional points (EPs) are inherently non-Hermitian band singularities [34], where both the eigenvalues and eigenvectors of different bands coalesce. Many interesting topological properties arise from EPs and have been shown to be the foundations of diverse promising applications [35–39]. From a codimension consideration, the order-two EPs can form stable exceptional lines (ELs) without the need for any symmetry in a three-dimensional (3D) parameter space, and the ELs can be further linked or knotted nontrivially [40–47]. However, as a typical EL configuration, the exceptional chain (EC) [48–50] formed by several connecting or osculating ELs is different from other EL morphologies because the stable existence of ECs demands symmetry protection. A recent study [50] has suggested that an EL can be assigned with an orientation determined by the complex-eigenvalue braiding around an EL, which is much similar to the right-hand rule describing the relation between dc electrical current and the magnetic fields it produces. The oriented ELs are source-free in the parameter space. It follows that stable ECs can exist as a consequence of the source-free principle of ELs in conjunction with certain symmetries, such as mirror, mirror-adjoint, and C_2T symmetries [49,50]. This interesting mechanism for stabilizing ECs has not yet been experimentally demonstrated or verified.

In this Letter, we study the stable existence of ECs using a non-Hermitian mechanical model with three synthetic dimensions. Unlike most non-Hermitian models that are based on Schrödinger-like first-order differential equations, the mechanical oscillators are described by second-order differential equations (SDEs) [51]. We reveal that SDEs can exhibit special non-Hermitian symmetries that become hidden after linearization to a Schrödinger-like Hamiltonian form, a process commonly employed in the study of topological mechanics [8,9]. Via generalizing the recently proposed notion of latent symmetries [52–54] to non-Hermitian scenarios, we demonstrate that these specific symmetries of the SDEs are essentially novel non-Hermitian latent symmetries of the linearized Hamiltonian, and they play a crucial role in protecting the stable ECs. By constructing mechanical oscillators with active components [55–57], we experimentally realize an EC and characterize its topological features. Our results not only demonstrate the unique properties of ECs but also highlight the distinctive potential of SDE systems in the future study of non-Hermitian physics.

SDE for non-Hermitian oscillators.—For a mechanical system consisting of N coupled harmonic oscillators, the dynamics is governed by the SDE [51]

$$\mathbf{M}\frac{d^2}{dt^2}X(t) = -\mathbf{K}X(t) - \mathbf{\Gamma}\frac{d}{dt}X(t), \tag{1}$$

wherein $X(t) = [x_1(t), x_2(t), \ldots, x_N(t)]^\intercal$ represents the displacements of N oscillators, and $\mathbf{M}$, $\mathbf{K}$, and $\mathbf{\Gamma}$ are real matrices representing the mass, stiffness, and damping matrices, respectively. $\mathbf{M}, \mathbf{\Gamma}$ are diagonal matrices, and $\mathbf{K}$ is symmetric (asymmetric) when the system is reciprocal (nonreciprocal). For time-harmonic solutions $x_i(t) = a_i e^{-i\omega t}$, the eigenfrequency ω obeys $Q(\omega)|\psi\rangle = (\omega^2\mathbf{M} - \mathbf{K} + i\omega\mathbf{\Gamma})|\psi\rangle = 0$, where $|\psi\rangle = (a_1, a_2, \ldots, a_N)^\intercal$ denotes the amplitudes of the oscillators and $Q(\omega)$ with real coefficient matrices is called a real quadratic matrix polynomial (QMP). The quadratic eigenvalue problem (QEP) for $Q(\omega)$ is to find right $|\psi_n^r\rangle$ and left $|\psi_n^l\rangle$ eigenvectors and an eigenfrequency ω_n satisfying

$$Q(\omega_n)|\psi_n^r\rangle = 0, \quad \langle\psi_n^l|Q(\omega_n) = 0. \tag{2}$$

Based on the customary approach in topological mechanics [8,9], the N-by-N QEP can be transformed to a $2N$-dimensional linear eigenvalue problem by a standard mathematical technique of reducing the order of SDEs [58]:

$$\mathcal{H}|\Psi_n\rangle = i\begin{pmatrix} \mathbf{0} & \mathbf{1} \\ -\mathbf{M}^{-1}\mathbf{K} & -\mathbf{M}^{-1}\mathbf{\Gamma} \end{pmatrix}|\Psi_n\rangle = \omega_n|\Psi_n\rangle$$

with $|\Psi_n\rangle = (|\psi_n^r\rangle, (d/dt)|\psi_n^r\rangle)^\intercal = (|\psi_n^r\rangle, -i\omega_n|\psi_n^r\rangle)^\intercal$, which takes the typical Hamiltonian formalism prevailing in tight-binding theories systems.

The real QMP of any mechanical system possesses an intrinsic symmetry $Q(\omega)^* = Q(-\omega^*)$, which indicates for any right eigenvector $|\psi_n^r\rangle$ satisfying Eq. (2), $|\psi_n^r\rangle^*$ is also a right eigenvector corresponding to the eigenvalue $-\omega_n^*$: $Q(-\omega_n^*)|\psi_n^r\rangle^* = 0$. Therefore, for an N-by-N real QEP with a real line gap at $\mathrm{Re}(\omega) = 0$, the $2N$ eigenvalues must come in pairs $(\omega_n, -\omega_n^*)$, implying that only N eigensolutions of the system are independent. Indeed, by linearization, this intrinsic symmetry of real QMP manifests as a particle-hole symmetry of the corresponding $2N$-dimensional Hamiltonian $\mathcal{H}$: $\mathcal{H}^* = -\mathcal{H}$ protecting the pairwise eigenvalues [7–9]. In the following, we focus on the upper N bands with $\mathrm{Re}(\omega_n) > 0$ because only the positive frequency (PF) modes are physically observable.

Theory of mechanical symmetry-protected ECs.—In a model with $N = 2$ [Fig. 1(a)], a nonreciprocal spring connects two nonconservative oscillators ($m_{1,2} = m_0$) subject to intrinsic damping and gain, respectively, and their motions are described by a two-by-two QMP, where the coefficient matrices can be expressed as $\mathbf{M} = \mathrm{diag}(m_0, m_0)$,

$$\mathbf{K} = \begin{pmatrix} \bar{\kappa}+\kappa/2 & -\chi \\ -\chi-\delta\chi & \bar{\kappa}-\kappa/2 \end{pmatrix}, \quad \mathbf{\Gamma} = \begin{pmatrix} \gamma/2 & 0 \\ 0 & -\gamma/2 \end{pmatrix}. \tag{3}$$

The diagonal terms of $\mathbf{K}$ determine the natural frequencies of the two isolated oscillators, and κ represents their

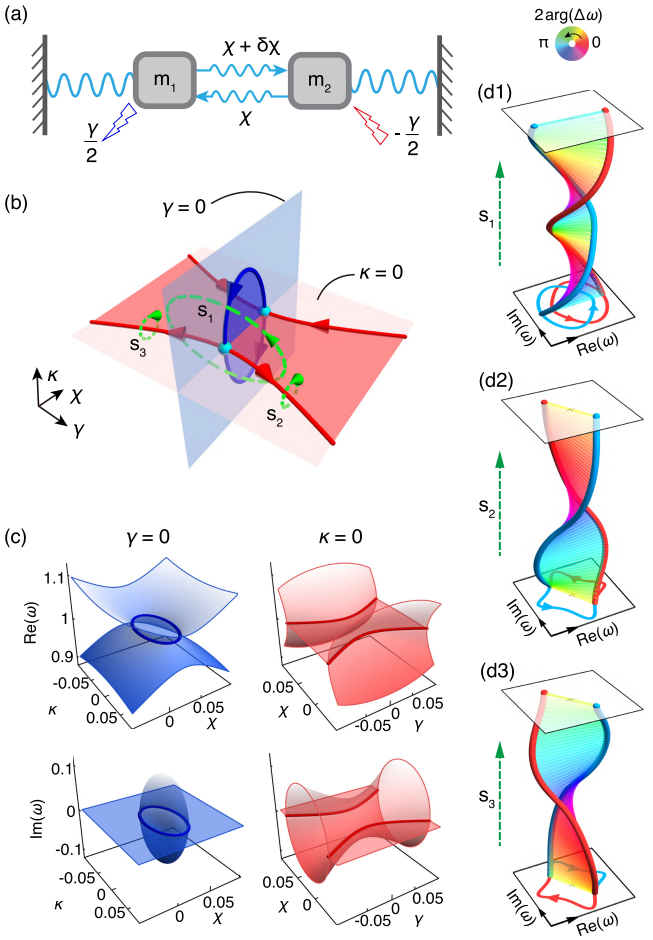

FIG. 1. (a) Schematic of the nonreciprocally coupled oscillator model. (b) An orthogonal EC formed by directed ELs in the 3D parameter space. (c) Eigenfrequencies of the two bands with positive real parts on planes $\gamma = 0$ and $\kappa = 0$. (d1)–(d3) Complex-eigenvalue braiding along the loops $S_{1,2,3}$ (green dashed lines) in (b), where the color of the bars connecting the two eigenfrequencies' trajectories represents twice the phase of the relative eigenfrequency $\Delta\omega = \omega_1 - \omega_2$. The fixed parameters used for plotting: $m_0 = \bar{\kappa} = 1$, $\delta\chi = -0.05$.

difference. The off-diagonal terms are different, which indicates nonreciprocal, direction-dependent coupling. The strictly opposite diagonal terms of $\mathbf{\Gamma}$ indicate balanced damping ($\gamma/2$) and gain ($-\gamma/2$) in the two oscillators.

We treat γ (relative damping), χ (coupling strength), and κ (on-site stiffness difference) as three synthetic dimensions spanning a 3D parameter space (γ, χ, κ) and keep $\bar{\kappa}$ and $\delta\chi$ fixed; the model possesses two symmetries in the parameter space [64]. The first is "γ symmetry" resulting from the balanced gain and loss of the two oscillators,

$$Q^*(\omega, \gamma) = Q(\omega^*, -\gamma). \tag{4}$$

Applying complex conjugate $\mathcal{K}$ on Eq. (2), we obtain $Q^*(\omega_n, \gamma)|\psi_n^r\rangle^* = Q(\omega_n^*, -\gamma)|\psi_n^r\rangle^* = 0$, indicating that for any eigenfrequency ω_n at γ, there is always a corresponding

eigenfrequency ω_n^* at $-\gamma$. It follows that the eigenfrequencies on the high-symmetry plane $\gamma = 0$ either take real values (outside the ring) or form complex conjugate pairs (inside the ring), as shown in the left panel of Fig. 1(c). In addition, the $\gamma = 0$ plane [Fig. 1(b)] is divided into exact (light blue) and broken (dark blue) phases by an exceptional ring (ER). We should note that when $\gamma = 0$, the non-Hermiticity of the system comes purely from the nonreciprocity $\delta\chi$, which determines the size of the ER.

In addition, since $\sigma_x \mathbf{K}^\dagger(\kappa)\sigma_x = \mathbf{K}(-\kappa)$, $\sigma_x \mathbf{\Gamma}^\dagger \sigma_x = -\mathbf{\Gamma}$ (σ_x is the first Pauli matrix), the QMP has a second "κ symmetry,"

$$\sigma_x Q^\dagger(\omega, \kappa)\sigma_x = Q(\omega^*, -\kappa). \tag{5}$$

Applying transpose conjugate on the QEP, we have $\langle\psi_n^r|Q^\dagger(\omega_n, \kappa) = \langle\psi_n^r|\sigma_x Q(\omega_n^*, -\kappa) = 0$ signifying that $\langle\psi_n^r|\sigma_x$ is a left eigenvector of $Q(\omega_n^*, -\kappa)$. Thus, for any eigenstate with frequency ω_n at κ, there is always an eigenstate with ω_n^* at $-\kappa$. On the high-symmetry plane $\kappa = 0$, the eigenvalues are either real or form complex conjugate pairs [right panel of Fig. 1(c)], and the ELs are fixed on the $\kappa = 0$ plane serving as the phase transition boundary between the exact (light red) and broken (dark red) phases [Fig. 1(b)]. Finally, under the protection of the symmetries (4) and (5), the ELs on two orthogonal planes connect together [cyan dots in Fig. 1(b)], forming a symmetry-protected EC in the 3D parameter space.

The γ symmetry (4) of $Q(\omega)$ can be mapped to an antiunitary symmetry of the four-by-four effective Hamiltonian $\mathcal{H}$: $U_\gamma \mathcal{H}(\gamma) U_\gamma^{-1} = \mathcal{H}(-\gamma)$ with $U_\gamma = \tau_z \otimes \sigma_0 \mathcal{K}$. However, the κ symmetry (5) cannot be directly transformed to a usual symmetry of $\mathcal{H}$. Rather, we revealed that it corresponds to a non-Hermitian latent symmetry of $\mathcal{H}$, i.e., $\sigma_x(\mathcal{H}(-\kappa)^n)_{\mathrm{BR}}\sigma_x = (\mathcal{H}(\kappa)^n)_{\mathrm{BR}}^\dagger$ for any $n \in \mathbb{N}$ with $(\mathcal{H}^n)_{\mathrm{BR}}$ denoting the bottom right block of $\mathcal{H}^n$ [58], which generalizes the notion of latent symmetry recently proposed in Hermitian systems [52–54]. This observation suggests that some symmetries of the original SDE become difficult to recognize in the effective Hamiltonian after linearization, and the origin of coalescence of eigenvalues becomes less obvious. Hence, directly analyzing the symmetries of the SDE is more natural in some scenarios for mechanical systems, though the effective Hamiltonian might be preferred for computational purposes. Moreover, the non-Hermitian latent symmetry also plays a significant role in characterizing the generalized crystalline symmetries appearing in non-Hermitian mechanical lattices (see Supplemental Materials [58] for details).

In non-Hermitian systems, when a pair of bands form EPs, their eigenvalues ω_m and ω_n will generally braid about each other along a loop S encircling the EPs [16,17]. To characterize this eigenvalue braiding, a half-quantized topological invariant called energy vorticity [13] has been introduced, $\nu_{mn}(S) = (1/2\pi)\oint_S d\mathbf{g} \cdot \nabla_{\mathbf{g}} \arg[\omega_m(\mathbf{g}) - \omega_n(\mathbf{g})]$. As shown in Figs. 1(d1)–1(d3), the eigenfrequency braiding of the two PF bands along the loop [dashed green lines in Fig. 1(b)] exhibits that twice the energy vorticity equals the net number of times the two bands braid. The energy vorticities carried by the loops are $\nu_{12}(S_1) = 1$, $\nu_{12}(S_2) = 1/2$, and $\nu_{12}(S_3) = -1/2$, respectively, where the sign of ν_{12} denotes the handedness of the braid and endows the encircled ELs with a positive orientation (which are indicated by arrows on ELs) in compliance with the right-hand rule [50]. For example, the positive (negative) sign of $\nu_{12}(S_2)$ [$\nu_{12}(S_3)$] indicates the EL has the same (reverse) direction as the rightward normal unit vector of the loop S_2 (S_3). And based on the direction of the ELs, we can prove a generalized source-free principle of the PF ELs in mechanical systems with the intrinsic particle-hole symmetry [50,58]: The number of PF ELs flowing into a junction must equal the number of PF ELs flowing out. This behavior is clearly observed for the oriented ELs near the chain points in

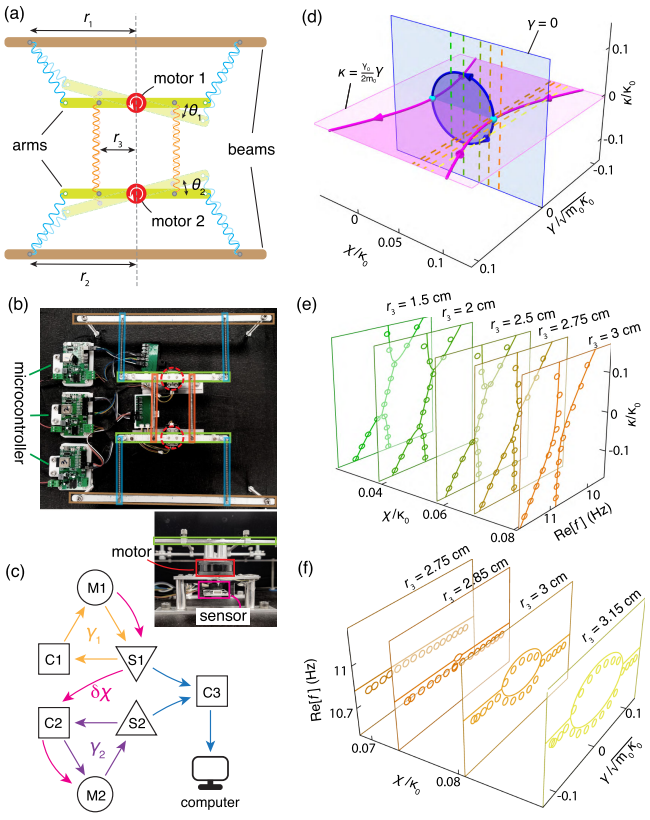

FIG. 2. (a) Schematic of the active oscillators. (b) Experimental setup. (c) Schematic of the control system where the microcontrollers (C1, C2) process the signals from the sensors (S1, S2) and send commands to the motors (M1, M2), and the instantaneous rotation angles of the motors are recorded by computer via the microcontroller C3. (d) EC realized by the experimental model, where an ER (blue tube) fixed on the plane $\gamma = 0$ connects two out-of-plane ELs (magenta tubes). The measured eigenfrequencies for different connection positions r_3 on the planes of (e) $\gamma = 0$ and (f) $\kappa = (\gamma_0/2m_0)\gamma$. The fixed parameters retrieved using the Green's function method: $\delta\chi = -0.073\kappa_0$, $\gamma_0/\sqrt{m_0\kappa_0} = 0.085$.

Fig. 1(b). It is noteworthy that the source-free principle is crucial for the stable existence of ECs. Specifically, it elucidates why the ELs constrained in distinct planes by the two symmetries must osculate each other, and further implies that the chain point is robust against the breaking of either symmetry [58].

Experimental realization of ECs.—Our experiment is performed using active mechanical oscillators. In the setup [Figs. 2(a)–2(c)], two rotational arms (green) connected to brushless dc motors (red) are attached to rigid beams (brown) at $r_{1,2}$ by two identical springs (blue). Another two identical springs (orange) separated by $2r_3$ connect the two rotational arms in parallel. At small-angle approximation $\sin(\theta_n) \approx \theta_n$, the vibration equations of the active oscillators are described by the SDE in Eq. (1), where $X(t) = [\theta_1(t), \theta_2(t)]^\intercal$ represents the oscillation angles of the two rotational arms with equal moments of inertia $\mathbf{M} = \mathrm{diag}(m_0, m_0)$, and the stiffness and damping matrices take the forms [58]

$$\mathbf{K} = \begin{pmatrix} \kappa_0 + \chi & -\chi \\ -\chi - \delta\chi & \kappa_0 - \kappa + \chi \end{pmatrix},$$
$$\mathbf{\Gamma} = \begin{pmatrix} \gamma_0 + \gamma/2 & 0 \\ 0 & \gamma_0 - \gamma/2 \end{pmatrix}. \tag{6}$$

$\mathbf{\Gamma}$ is loss biased by adding a constant loss γ_0 to avoid instability issues encountered when the system is in the gain regime. The parameters χ, κ_0, and $(\kappa_0 - \kappa)$ are determined by conservative torques applied by the orange springs, the upper blue springs, and the lower blue springs in Fig. 2(a), respectively. The parameters $\delta\chi$ and γ are implemented as nonconservative torques exerted by the motors. To this end, the instantaneous oscillation angle is measured using a Hall sensor in real time. The angle is used as feedback to drive the microcontrollers that are programmed to command the motors to exert the desired torques [see Fig. 2(b)].

During the experiments, κ_0 is kept constant by fixing r_1, and κ and χ are tuned by changing r_2 and r_3, respectively. γ and $\delta\chi$ are tuned by velocity-dependent and angle-dependent torques applied to the motors (see details in [58]), as shown in Fig. 2(c). Compared with the theoretical model in Fig. 1, the biased loss γ_0 reduces the whole-space γ symmetry shown by Eq. (4) to a subspace symmetry on the $\gamma = 0$ plane in the experimental system:

$$Q^*(\omega) = Q(\omega^* - i\gamma_0/m_0). \tag{7}$$

Meanwhile, the κ symmetry in Eq. (5) is reduced to a subspace symmetry on the oblique plane $\kappa = (\gamma_0/2m_0)\gamma$ [58]:

$$\sigma_x Q^\dagger(\omega)\sigma_x = Q(\omega^* - i\gamma_0/m_0), \tag{8}$$

which can be regarded as a non-Hermitian latent symmetry for the linearized Hamiltonian of the QMP on that plane. Remarkably, the two subspace symmetries can also guarantee that the eigenfrequencies on the two planes either appear in pairs $(\omega_n, \omega_n^* - i\gamma_0/m_0)$ or have a common imaginary part $-i\gamma_0/2m_0$ corresponding to the broken and exact phases, respectively. Accordingly, despite the presence of background loss, ELs are still rigorously fixed at the boundaries of the two phases on the two planes and are joined on their intersection line $\gamma = \kappa = 0$, hence forming an EC.

In Fig. 2(d), we plot the EC configuration of the experimental model with a fixed nonreciprocal strength $\delta\chi = -0.073\kappa_0$, which is retrieved using the Green's function method [58]. The inclination of the $\kappa = (\gamma_0/2m_0)\gamma$

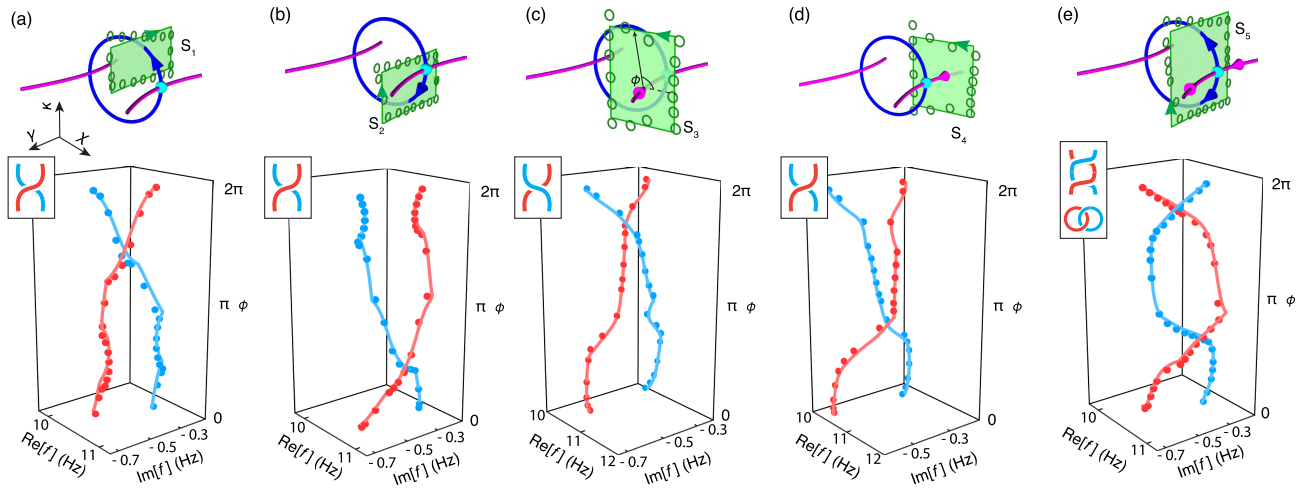

FIG. 3. Complex eigenfrequency braiding (red and cyan lines and dots in the lower panels) along rectangular green loops, (a) S_1, (b) S_2, (c) S_3, (d) S_4, and (e) S_5, encircling different ELs, where $\phi \in [0, 2\pi]$ represents the sweeping parameter of the loops. The braiding diagrams are plotted in the insets. The details about the parameters retrieval can be found in Ref. [58].

plane (magenta) is about 2.5° in the figure due to the small value of γ_0 in the experiments. Figures 2(e) and 2(f) display the measured eigenfrequencies of the PF bands for varying χ [dashed lines in Fig. 2(d)] on the $\gamma = 0$ and $\kappa = (\gamma_0/2m_0)\gamma$ planes. The EPs can be clearly identified from the measured band structures, and the EC formed by the ELs on the two planes becomes obvious by tracing the positions of the EPs.

By measuring eigenfrequency braidings, we experimentally verified the orientations of the ELs assigned in Fig. 2(d) and validated the formation of the EC. As shown in Figs. 3(a) and 3(b), we varied the parameters γ and κ along two rectangular clockwise loops encircling the upper and lower semi-ER on the plane $\chi = 0.057\kappa_0$. The measured eigenfrequency braidings along the loops are shown in the lower panels, from which the energy vorticities are obtained as $\nu_{12}(S_1) = \nu_{12}(S_2) = 1/2$. According to the right-hand rule, the upper and lower semi-ERs both flow outward from the chain point (cyan dot). As shown in Figs. 3(c) and 3(d), we chose another two loops S_3 and S_4 on the planes of $\gamma/\sqrt{m_0\kappa_0} = 0.043$ and of $\gamma/\sqrt{m_0\kappa_0} = -0.03$. The nontrivial eigenfrequency braiding implies the presence of an EL enclosed in each loop, and the orientations of the ELs are both toward the chain point as per the signs of energy vorticities $\nu_{12}(S_3) = -1/2$ and $\nu_{12}(S_4) = 1/2$, which confirms the source-free principle at the chain points. Lastly, we consider a loop encircling the chain point (cyan dot) shown in Fig. 3(e), and find the eigenfrequencies braid twice, which form a Hopf link after connecting the eigenfrequency trajectories head to tail.

Discussion.—We have also studied the physical effect induced by the ECs in 3D mechanical lattices and have discovered that the unique concurrent linear intersections of the real and imaginary parts of bands near the EC point can give rise to the exotic phenomenon of splitting and reshaping a spatially localized pulse into two oppositely propagating needle pulses [58]. This discovery demonstrates that ECs also possess functional properties with promising application potential.

In summary, we revealed that the non-Hermitian latent symmetries intrinsic to SDE governing mechanical systems play a pivotal role in the formation of ECs, and such a symmetry-protected EC is experimentally confirmed using coupled active mechanical oscillators. By measuring the eigenfrequency braiding around ELs, we identified the orientations of the ELs and verified the generalized source-free principle for the PF ELs in SDE problems. Our Letter not only demonstrates the stable existence of an EC as a different kind of topological configuration, but also opens the door to the topological effects inherent to the SDEs, which govern a broad class of systems encompassing classical mechanics, classical waves, electricity [65–67], optomechanical [68], and microelectromechanical [69] systems.

We thank Professor Zhao-Qing Zhang, Dr. Hongwei Jia, Dr. Jing Hu, and Dr. Yixin Xiao for helpful discussions. This work is supported by the National Key R&D Program of China (Grant No. 2022YFA1404400), the Research Grants Council of Hong Kong (Grants No. AoE/P-502/20, No. R6015-18, No. RFS2223-2S01, No. 16310422, No. 12302420, and No. 12301822), and the Croucher Foundation (Grant No. CAS20SC01).

*These authors contributed equally to this work.
†phgcma@hkbu.edu.hk
‡phchan@ust.hk

[1] M. Z. Hasan and C. L. Kane, Colloquium: Topological insulators, Rev. Mod. Phys. **82**, 3045 (2010).
[2] X.-L. Qi and S.-C. Zhang, Topological insulators and superconductors, Rev. Mod. Phys. **83**, 1057 (2011).
[3] L. Lu, J. D. Joannopoulos, and M. Soljačić, Topological photonics, Nat. Photonics **8**, 821 (2014).
[4] T. Ozawa, H. M. Price, A. Amo, N. Goldman, M. Hafezi, L. Lu, M. C. Rechtsman, D. Schuster, J. Simon, O. Zilberberg, and I. Carusotto, Topological photonics, Rev. Mod. Phys. **91**, 015006 (2019).
[5] G. Ma, M. Xiao, and C. T. Chan, Topological phases in acoustic and mechanical systems, Nat. Rev. Phys. **1**, 281 (2019).
[6] H. Xue, Y. Yang, and B. Zhang, Topological acoustics, Nat. Rev. Mater. **7**, 974 (2022).
[7] C. L. Kane and T. C. Lubensky, Topological boundary modes in isostatic lattices, Nat. Phys. **10**, 39 (2014).
[8] R. Süsstrunk and S. D. Huber, Classification of topological phonons in linear mechanical metamaterials, Proc. Natl. Acad. Sci. U.S.A. **113**, E4767 (2016).
[9] T. Yoshida and Y. Hatsugai, Exceptional rings protected by emergent symmetry for mechanical systems, Phys. Rev. B **100**, 054109 (2019).
[10] P. Wang, L. Lu, and K. Bertoldi, Topological phononic crystals with one-way elastic edge waves, Phys. Rev. Lett. **115**, 104302 (2015).
[11] R. Süsstrunk and S. D. Huber, Observation of phononic helical edge states in a mechanical topological insulator, Science **349**, 47 (2015).
[12] M. Fruchart, Y. Zhou, and V. Vitelli, Dualities and non-Abelian mechanics, Nature (London) **577**, 636 (2020).
[13] H. Shen, B. Zhen, and L. Fu, Topological band theory for non-Hermitian Hamiltonians, Phys. Rev. Lett. **120**, 146402 (2018).
[14] K. Kawabata, K. Shiozaki, M. Ueda, and M. Sato, Symmetry and topology in non-Hermitian physics, Phys. Rev. X **9**, 041015 (2019).
[15] K. Kawabata, T. Bessho, and M. Sato, Classification of exceptional points and non-Hermitian topological semimetals, Phys. Rev. Lett. **123**, 066405 (2019).
[16] C. C. Wojcik, X.-Q. Sun, T. Bzdušek, and S. Fan, Homotopy characterization of non-Hermitian Hamiltonians, Phys. Rev. B **101**, 205417 (2020).
[17] K. Wang, A. Dutt, C. C. Wojcik, and S. Fan, Topological complex-energy braiding of non-Hermitian bands, Nature (London) **598**, 59 (2021).
[18] H. Hu and E. Zhao, Knots and non-Hermitian Bloch bands, Phys. Rev. Lett. **126**, 010401 (2021).

[19] Z. Yang, A. P. Schnyder, J. Hu, and C.-K. Chiu, Fermion doubling theorems in two-dimensional non-Hermitian systems for Fermi points and exceptional points, Phys. Rev. Lett. **126**, 086401 (2021).
[20] K. Ding, G. Ma, M. Xiao, Z. Q. Zhang, and C. T. Chan, Emergence, coalescence, and topological properties of multiple exceptional points and their experimental realization, Phys. Rev. X **6**, 021007 (2016).
[21] M. Brandenbourger, X. Locsin, E. Lerner, and C. Coulais, Non-reciprocal robotic metamaterials, Nat. Commun. **10**, 4608 (2019).
[22] W. Tang, X. Jiang, K. Ding, Y.-X. Xiao, Z.-Q. Zhang, C. T. Chan, and G. Ma, Exceptional nexus with a hybrid topological invariant, Science **370**, 1077 (2020).
[23] A. Ghatak, M. Brandenbourger, J. van Wezel, and C. Coulais, Observation of non-Hermitian topology and its bulk-edge correspondence in an active mechanical metamaterial, Proc. Natl. Acad. Sci. U.S.A. **117**, 29561 (2020).
[24] W. Tang, K. Ding, and G. Ma, Direct measurement of topological properties of an exceptional parabola, Phys. Rev. Lett. **127**, 034301 (2021).
[25] L. Zhang, Y. Yang, Y. Ge, Y.-J. Guan, Q. Chen, Q. Yan, F. Chen, R. Xi, Y. Li, D. Jia, S.-Q. Yuan, H.-X. Sun, H. Chen, and B. Zhang, Acoustic non-Hermitian skin effect from twisted winding topology, Nat. Commun. **12**, 6297 (2021).
[26] H. Gao, H. Xue, Z. Gu, T. Liu, J. Zhu, and B. Zhang, Non-Hermitian route to higher-order topology in an acoustic crystal, Nat. Commun. **12**, 1888 (2021).
[27] X. Zhang, Y. Tian, J.-H. Jiang, M.-H. Lu, and Y.-F. Chen, Observation of higher-order non-Hermitian skin effect, Nat. Commun. **12**, 5377 (2021).
[28] B. Hu, Z. Zhang, H. Zhang, L. Zheng, W. Xiong, Z. Yue, X. Wang, J. Xu, Y. Cheng, X. Liu, and J. Christensen, Non-Hermitian topological whispering gallery, Nature (London) **597**, 655 (2021).
[29] W. Tang, K. Ding, and G. Ma, Experimental realization of non-Abelian permutations in a three-state non-Hermitian system, Natl. Sci. Rev. **9**, nwac010 (2022).
[30] P. Baconnier, D. Shohat, C. H. López, C. Coulais, V. Démery, G. Düring, and O. Dauchot, Selective and collective actuation in active solids, Nat. Phys. **18**, 1234 (2022).
[31] J.-J. Liu, Z.-W. Li, Z.-G. Chen, W. Tang, A. Chen, B. Liang, G. Ma, and J.-C. Cheng, Experimental realization of Weyl exceptional rings in a synthetic three-dimensional non-Hermitian phononic crystal, Phys. Rev. Lett. **129**, 084301 (2022).
[32] Q. Zhang, Y. Li, H. Sun, X. Liu, L. Zhao, X. Feng, X. Fan, and C. Qiu, Observation of acoustic non-Hermitian Bloch braids and associated topological phase transitions, Phys. Rev. Lett. **130**, 017201 (2023).
[33] W. Tang, K. Ding, and G. Ma, Realization and topological properties of third-order exceptional lines embedded in exceptional surfaces, Nat. Commun. **14**, 6660 (2023).
[34] W. D. Heiss, Exceptional points of non-Hermitian operators, J. Phys. A **37**, 2455 (2004).
[35] M.-A. Miri and A. Alù, Exceptional points in optics and photonics, Science **363**, aar7709 (2019).
[36] Ş. K. Özdemir, S. Rotter, F. Nori, and L. Yang, Parity-time symmetry and exceptional points in photonics, Nat. Mater. **18**, 783 (2019).
[37] S. Shankar, A. Souslov, M. J. Bowick, M. C. Marchetti, and V. Vitelli, Topological active matter, Nat. Rev. Phys. **4**, 380 (2022).
[38] E. J. Bergholtz, J. C. Budich, and F. K. Kunst, Exceptional topology of non-Hermitian systems, Rev. Mod. Phys. **93**, 015005 (2021).
[39] K. Ding, C. Fang, and G. Ma, Non-Hermitian topology and exceptional-point geometries, Nat. Rev. Phys. **4**, 745 (2022).
[40] J. Carlström and E. J. Bergholtz, Exceptional links and twisted Fermi ribbons in non-Hermitian systems, Phys. Rev. A **98**, 042114 (2018).
[41] Z. Yang and J. Hu, Non-Hermitian Hopf-link exceptional line semimetals, Phys. Rev. B **99**, 081102(R) (2019).
[42] Z. Zhang, Z. Yang, and J. Hu, Bulk-boundary correspondence in non-Hermitian Hopf-link exceptional line semimetals, Phys. Rev. B **102**, 045412 (2020).
[43] P. He, J.-H. Fu, D.-W. Zhang, and S.-L. Zhu, Double exceptional links in a three-dimensional dissipative cold atomic gas, Phys. Rev. A **102**, 023308 (2020).
[44] J. Carlström, M. Stålhammar, J. C. Budich, and E. J. Bergholtz, Knotted non-Hermitian metals, Phys. Rev. B **99**, 161115(R) (2019).
[45] C. H. Lee, A. Sutrisno, T. Hofmann, T. Helbig, Y. Liu, Y. S. Ang, L. K. Ang, X. Zhang, M. Greiter, and R. Thomale, Imaging nodal knots in momentum space through topolectrical circuits, Nat. Commun. **11**, 4385 (2020).
[46] X. Zhang, G. Li, Y. Liu, T. Tai, R. Thomale, and C. H. Lee, Tidal surface states as fingerprints of non-Hermitian nodal knot metals, Commun. Phys. **4**, 47 (2021).
[47] K. Wang, L. Xiao, J. C. Budich, W. Yi, and P. Xue, Simulating Exceptional non-Hermitian metals with single-photon interferometry, Phys. Rev. Lett. **127**, 026404 (2021).
[48] A. Cerjan, M. Xiao, L. Yuan, and S. Fan, Effects of non-Hermitian perturbations on Weyl Hamiltonians with arbitrary topological charges, Phys. Rev. B **97**, 075128 (2018).
[49] Q. Yan, Q. Chen, L. Zhang, R. Xi, H. Chen, and Y. Yang, Unconventional Weyl exceptional contours in non-Hermitian photonic continua, Photonics Res. **9**, 2435 (2021).
[50] R.-Y. Zhang, X. Cui, W.-J. Chen, Z.-Q. Zhang, and C. T. Chan, Symmetry-protected topological exceptional chains in non-Hermitian crystals, Commun. Phys. **6**, 169 (2023).
[51] F. Tisseur and K. Meerbergen, The quadratic eigenvalue problem, SIAM Rev. **43**, 235 (2001).
[52] M. Röntgen, M. Pyzh, C. V. Morfonios, N. E. Palaiodimopoulos, F. K. Diakonos, and P. Schmelcher, Latent symmetry induced degeneracies, Phys. Rev. Lett. **126**, 180601 (2021).
[53] C. V. Morfonios, M. Röntgen, M. Pyzh, and P. Schmelcher, Flat bands by latent symmetry, Phys. Rev. B **104**, 035105 (2021).
[54] M. Röntgen, C. V. Morfonios, P. Schmelcher, and V. Pagneux, Hidden symmetries in acoustic wave systems, Phys. Rev. Lett. **130**, 077201 (2023).
[55] W. Wang, X. Wang, and G. Ma, Non-Hermitian morphing of topological modes, Nature (London) **608**, 50 (2022).
[56] W. Wang, X. Wang, and G. Ma, Extended state in a localized continuum, Phys. Rev. Lett. **129**, 264301 (2022).
[57] W. Wang, M. Hu, X. Wang, G. Ma, and K. Ding, Experimental realization of geometry-dependent skin effect

in a reciprocal two-dimensional lattice, Phys. Rev. Lett. **131**, 207201 (2023).

[58] See Supplemental Materials at http://link.aps.org/supplemental/10.1103/PhysRevLett.131.237201, which includes Refs. [59–63], for (i) the proof of the generalized source-free principle for PF ELs, (ii) discussion on the topological nature of ECs, (iii) non-Hermitian latent symmetry, (iv) effective two-level tight-binding model, (v) experimental and measurement details, and (vi) physical effect induced by the EC in a 3D mechanical lattice.

[59] T. Kato, *Perturbation Theory for Linear Operators*, 3rd ed. (Springer-Verlag, Berlin, 1995).

[60] J. Wang, W. Chen, and Q. Zhan, Engineering of high purity ultra-long optical needle field through reversing the electric dipole array radiation, Opt. Express **18**, 21965 (2010).

[61] K. J. Parker and M. A. Alonso, Longitudinal iso-phase condition and needle pulses, Opt. Express **24**, 28669 (2016).

[62] R. Grunwald and M. Bock, Needle beams: A review, Adv. Phys. **5**, 1736950 (2020).

[63] R. Cao, J. Zhao, L. Li, L. Du, Y. Zhang, Y. Luo, L. Jiang, S. Davis, Q. Zhou, A. de la Zerda, and L. V. Wang, Optical-resolution photoacoustic microscopy with a needle-shaped beam, Nat. Photonics **17**, 89 (2023).

[64] Note that the SDE for our system can be reduced to a two-level tight-binding model in the quasidegenerate approximation, and the γ and κ symmetries for the SDE are mapped to the crystalline C_2T and mirror-adjoint symmetries for the effective model (see details in [58]).

[65] T. Helbig, T. Hofmann, S. Imhof, M. Abdelghany, T. Kiessling, L. W. Molenkamp, C. H. Lee, A. Szameit, M. Greiter, and R. Thomale, Generalized bulk-boundary correspondence in non-Hermitian topolectrical circuits, Nat. Phys. **16**, 747 (2020).

[66] S. Liu, R. Shao, S. Ma, L. Zhang, O. You, H. Wu, Y. J. Xiang, T. J. Cui, and S. Zhang, Non-Hermitian skin effect in a non-Hermitian electrical circuit, Research **2021**, 5608038 (2021).

[67] J. Hu, R.-Y. Zhang, Y. Wang, X. Ouyang, Y. Zhu, H. Jia, and C. T. Chan, Non-Hermitian swallowtail catastrophe revealing transitions across diverse topological singularities, Nat. Phys. **19**, 1098 (2023).

[68] X. Li, Y. Liu, Z. Lin, J. Ng, and C. T. Chan, Non-Hermitian physics for optical manipulation uncovers inherent instability of large clusters, Nat. Commun. **12**, 6597 (2021).

[69] Z. Xu, X. Gao, J. Bang, Z. Jacob, and T. Li, Non-reciprocal energy transfer through the Casimir effect, Nat. Nanotechnol. **17**, 148 (2022).